Coupled molecular-dynamics Monte Carlo study of the transport properties of lateral surface superlattices

Toshishige Yamada and D. K. Ferry
Center for Solid State Electronics Research, Arizona State University, Tempe, Arizona 85287-6206
(Received 20 April 1992; revised manuscript received 22 October 1992)

The transport properties of a lateral surface superlattice, a two-dimensional (2D) electron system in a 2D periodic potential, are studied with a molecular-dynamics Monte Carlo technique including the Coulomb interaction. Excellent numerical energy conservation is achieved by adopting a predictor-corrector algorithm to integrate the equations of motion. With increasing 2D potential amplitude, electrons show a transition, from a mobile phase to an immobile phase, where the radial distribution function has some characteristic peaks, indicating the beginning of the long-range ordering of the electrons in the potential minima. The velocity autocorrelation function shows a 2D plasma oscillation in the mobile phase, while in the immobile phase the classical oscillation at the bottom of the potential well is observed. Raising the temperature improves the transport since electrons are released from the constraint of the 2D potential and the Coulomb potential.

I. INTRODUCTION

Due to the rapid progress in semiconductor technology, a two-dimensional (2D) electron gas in a 2D periodic potential with the period $a \sim 0.1\ \mu$m can now be achieved in lateral surface superlattices (LSSL's) forming field-effect-transistor (FET) structures with meshed-gate electrodes. Transport properties of this system have been studied extensively both experimentally and theoretically.[1,2] A classical electron picture often gives a successful explanation of the experimental results at temperatures above liquid helium.[3–5]

However, most such studies have focused on a situation where the number of electrons in a unit cell is so large that the Coulomb interaction between electrons is well screened, and, as a result, a noninteracting, independent electron picture prevails. If we reduce the number of electrons in a unit cell so that the Fermi energy becomes on the order of the thermal energy 4.2 K, the role of the Pauli exclusion principle is more irrelevant, and the Coulomb interaction is no longer well screened. All the electrons are more or less bound to one another through the Coulomb interaction. The motion of a certain electron affects that of other electrons and provides feedback to the original electron. In thermal equilibrium without the Coulomb interaction, electrons prefer to stay near the bottom of the 2D potential well and the typical separation of electrons would be $d \sim a/10 \sim 0.01\ \mu$m for a potential depth $\sim 10 k_B T$. This small separation causes an unscreened Coulomb energy $e^2/(4\pi\varepsilon d)$ as large as ~ 11 meV for a pair of electrons in a GaAs channel. At 4.2 K, this value is much larger than the thermal energy and electrons are driven apart some reasonable distance in the Coulomb interaction, although this increases the average 2D potential energy of electrons. Therefore, the role of the Coulomb interaction is essential in the LSSL if the number of electrons in a unit cell is small so that the screening is weak. The transport properties should be profoundly influenced by the Coulomb interaction.

We study the effect of the Coulomb interaction on transport properties in LSSL structures with a molecular-dynamics technique,[6] which is a straightforward method to include the Coulomb interaction. At each time step, the Coulomb force is calculated for all the pairs of electrons and their positions and momenta are updated according to this force. The advantage of this method is that it makes no assumptions for screening or collective-mode excitations such as the plasma oscillation. These effects are automatically included in molecular dynamics. In order to eliminate unwanted effects from the use of the finite number of electrons in simulations, periodic boundary conditions are adopted which enable us to simulate an infinitely large system. Thermal equilibrium is assumed in all the simulations here, and the diffusion constant is evaluated by the temporal derivative of an Einstein plot, i.e., the plot of the mean-square displacement of electrons versus time. Scattering by both impurity and phonons is also included in the simulation with a usual Monte Carlo technique, although impurity scattering dominates at this low temperature.

Phonon scattering is infrequent on the time scale of interest, and the number of electrons is fixed so that the system is isolated. Thus the total energy of electrons, which is the summation of kinetic energy, 2D potential energy, and Coulomb energy has to be conserved (even with phonon emission/absorption, the energy conservation can be extended to include the phonon energy transfer). In this situation, achieving good numerical energy conservation is necessary in the present molecular dynamics. We have used a predictor-corrector method to integrate the equations of motion and succeeded in achieving five-digit numerical energy conservation. In Sec. II, the model and the numerical techniques are explained, and in Sec. III the results and discussion are given. The conclusion is given in Sec. IV.

II. SIMULATION METHOD

The electrons are considered as classical pointlike particles rather than quantum-mechanical waves, which

 ©1993 The American Physical Society

move in the 2D potential created in a GaAs LSSL structure by $V(x,y)=V_0[\cos(2\pi x/a)+\cos(2\pi y/a)+2]/4$ with $a=0.16$ μm, following the experiment.[2] The potential amplitude V_0 is varied from 0 to 40 meV. The temperature is assumed to be 4.2 K and realistic impurity and phonon scattering is included in the ensemble Monte Carlo method as discrete events, although the impurity scattering dominates at this temperature. The electron areal density is 1.4×10^{10} cm^{-2} and the Fermi wave vector and the Fermi energy are 3.0×10^5 cm^{-1} and 0.39 meV, respectively, with a parabolic-band assumption. Since the Fermi energy is on the order of the thermal energy 0.36 meV, the role of the Pauli exclusion principle is not important, and we use a classical particle picture.[7] On the other hand, because of the low areal density the screening is weak and the role of the Coulomb interaction is essential in the present case,[8] as was discussed in the previous section. The effect of the Coulomb interaction is included in the electron dynamics itself through molecular dynamics, and the energy band is assumed to remain parabolic.

We have used a combination of a Monte Carlo technique and a molecular dynamics[6] to simulate the present situation. Electrons perform a free flight under the influence of the potentials and, if scattering occurs, they suddenly change their momentum (and energy in inelastic processes) and start another free flight. The scattering is a stochastic process, and whether or not it occurs is determined in the usual Monte Carlo code with the help of random numbers. We adopt an envelope function[9] corresponding to the lowest stubband in the FET channel and evaluate the scattering rates in the quasi-two-dimensional inversion channel based on the scattering rates formulated by Price.[10] The Coulomb interaction between electrons is treated through a molecular-dynamics technique. This treatment is markedly different from that of impurity or phonon scattering. We do not treat it as a discrete scattering event, but as a continuous one. At each time step, the Coulomb force is calculated for all electrons and this is used to update the position and momentum of each electron during the subsequent time step. In this way, we include various many-body effects automatically without using any artificial assumptions for the screening or the collective excitation mode. Although impurity and phonon scattering are included in the Monte Carlo part of the simulation for completeness, the Coulomb interaction dominates the dynamics of the system and the scattering gives only a small perturbation, as will be discussed later.

In order to eliminate unwanted boundary effects due to the finite number of electrons used, a periodic boundary condition is employed which enables us to simulate virtually an infinitely large system. We typically simulate 32 electrons in 3×3 unit cells, corresponding to electron areal density 1.4×10^{10} cm^{-2}, and the periodic boundary condition is imposed for this square area with the side length $L=3a$. When an electron leaves the square crossing by the boundary $x=L$, another electron is input from the equivalent boundary $x=0$ with the same y coordinate and the same momentum. The number of the electrons in the square remains the same throughout the simulation. Thus, the dynamics is *topologically* equivalent to that of electrons distributed on a torus surface since $x=0$ and $x=L$ are equivalent and $y=0$ and $y=L$ are equivalent, respectively.[11]

The Coulomb interaction has to be consistently defined with the periodic boundary condition so that the total energy is conserved. Usual techniques to truncate the interaction for a pair of electrons with a distance longer than a certain cutoff length are not appropriate. The first reason is that the long-range nature of the Coulomb interaction behaves as r^{-1} and prohibits a natural definition of the cutoff length. The second is that the number of interacting electrons may change with time in the truncation process, leading to an abrupt, unphysical change in total energy. The most appropriate formulation of the Coulomb interaction consistent with the periodic boundary condition is related to the Ewald sum method.[12] In this method, an electron is considered to interact with other electrons in the square and also with all electron images in the replicas of the square.

However, the implementation of the exact Ewald sum is unreasonably time consuming since the Coulomb potential in the Ewald form cannot be expressed in a closed analytical form and needs an extensive numerical 2D integration, which is often subject to numerical errors. In practice, we need to decide which to take: the exact Ewald sum formalism but with a poor numerical energy conservation or an approximated Ewald sum in a simple analytical form with an excellent numerical energy conservation within the approximation. Here we have chosen the latter and employed a minimum image approximation for the Ewald sum,[11,13] where an electron is assumed to interact with $N-1$ other electrons in the square through specially defined distances. The distance of electrons i and j in the minimum image approximation is given by the length of the minimum image vector $\mathbf{r}_{ij}$ defined as follows. Let $\mathbf{a}_x=(L,0)$ and $\mathbf{a}_y=(0,L)$. Then $\mathbf{r}_{ij}=\mathbf{x}_j-\mathbf{x}_i-n_x\mathbf{a}_x-n_y\mathbf{a}_y$, where n_x and n_y are chosen to be the integers to minimize the length $|\mathbf{r}_{ij}|$.

The minimum image approximation can be understood using an analogy to the dynamics with N electrons distributed on a torus surface, as remarked above. The approximation assumes that an electron always interacts with $N-1$ other electrons on the torus surface with a specially defined distance. There are in general plural paths along the surface to connect two electrons, as shown in Fig. 1. The electrons are assumed to interact with one another through the distance defined by the length of the shortest path, which corresponds to the formation of the minimum image vector. This is a *topologically* equivalent definition of the distance above, neglecting the curvature of the torus. When electron i or j crosses the axis $x=L$, the integer n_x to give the minimum image vector $\mathbf{r}_{ij}$ changes by unity, but the distance itself remains the same, causing no artificial change in the Coulomb energy. Thus the minimum image approximation satisfies two requirements: it does not break the energy conservation law, and it has an electron interact with the same number of electrons throughout the simulation.

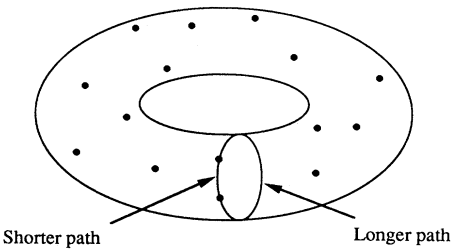

FIG. 1. Electron dynamics on a torus. This is topologically equivalent to the dynamics with the periodic boundary condition applied to the square simulation area within the minimum image approximation. The shorter path corresponds to the minimum image vector, and it determines the distance of two particles used in the evaluation of the Coulomb force.

The minimum image approximation has an important translational symmetry that the original Ewald sum also had, which is that the Coulomb potential of an electron does not change under a spatial translation of all the electrons by the amount of lattice vectors. Therefore, the minimum image approximation is considered as the simplest possible approximation for the Ewald sum to retain the translational property of the Ewald sum, and is *completely different* from a usual simple truncation of the potential, which does not retain it. The validity of this approximation will be examined in the next section by determining the 2D plasma frequency. The frequency represents the nature of the long-wavelength limit of the Coulomb interaction and seems best suitable to check whether or not an artificial truncation effect is introduced. It will turn out that the present prescription supports a 2D plasma frequency that tracks properly for two different electron densities, and gives results in keeping with those obtained by more extensive plasma calculations.

A remark has to be made that the origin of the Coulomb energy must be properly adjusted in the minimum image approximation if we are interested in the internal energy of the system. In the exact Ewald sum formalism, a uniform background charge, required to neutralize the electron negative charge, is assumed, and the result of the Ewald sum can be used directly to evaluate the internal energy. In the minimum image approximation, however, we need to make a correction to the energy origin by adding some constant value since the effect of the background charge is not included. In the results below, this constant value has always been chosen to be zero in the evaluation of the Coulomb energy.

The Coulomb potential is now written with a simple form in the minimum image approximation. In molecular dynamics, we update the position x and momentum p by

$$x(i+1)=x(i)+\int_0^{\Delta t} p\ dt\ , \tag{1}$$

$$p(i+1)=p(i)+\int_0^{\Delta t} f\ dt\ , \tag{2}$$

where $x(i)$ and $p(i)$ indicate the functional values of $x(t)$ and $p(t)$ at the ith time step with step period Δt, and f is the force (in the units of $m=1$). The force f is generally a complicated function of positions (and momenta) of all electrons: the force from the 2D potential is a function of the position of an electron, and the Coulomb force is a function of the positions of all electrons. Using a trapezoidal formula to approximate the integrals, we have

$$x(i+1)=x(i)+[p(i)+p(i+1)]\Delta t/2\ , \tag{3}$$

$$p(i+1)=p(i)+[f(i)+f(i+1)]\Delta t/2\ , \tag{4}$$

where the two functional values at i and $i+1$ are used to evaluate each integration. This is a self-consistent equation. By assuming $p(i+1)$, (3) gives $x(i+1)$. Then $f(i+1)$ is determined from $x(i+1)$ and $p(i+1)$. By knowing $f(i+1)$, (4) gives $p(i+1)$, and this has to be self-consistent with the original value of $p(i+1)$ that we started from. The determination of $x(i+1)$ and $p(i+1)$ to satisfy this self-consistency at each time step leads to an excellent numerical energy conservation.

This kind of self-consistent equation can be solved by the iteration or the predictor-corrector method.[12] The first prediction is

$$f(i+1)=f(i)\ . \tag{5}$$

Then we have

$$p'(i+1)=p(i)+f(i)\Delta t\ , \tag{6}$$

$$x'(i+1)=x(i)+[p(i)+p'(i+1)]\Delta t/2\ . \tag{7}$$

We can correct the first predicted position and momentum, since the corrected force $f'(i+1)$ can be calculated using $x'(i+1)$ and $p'(i+1)$. Then,

$$p''(i+1)=p(i)+[f(i)+f'(i+1)]\Delta t/2\ , \tag{8}$$

$$x''(i+1)=x(i)+[p(i)+p'(i+1)]\Delta t/2\ . \tag{9}$$

This procedure is repeated until good convergence is obtained, but adopting $p''(i+1)$ and $x''(i+1)$ is enough in the present simulations. Actually, adopting p'' and x'' leads to five-digit accuracy in energy conservation throughout typical simulations up to $\sim 10^2$ ps with the Coulomb interaction.

The implementation of this predictor-corrector method in the Monte Carlo program needs some care, since we have two time periods corresponding to Δt. One is the time duration t_m for molecular dynamics, which is constant over the simulation, and the second is the free flight time t_f between scattering, which is a random variable. An electron performs a free flight during the time period $\min(t_m,t_f)$ and in most cases this is equal to t_m, since t_m is chosen to be much shorter than the relaxation time. The Coulomb force is updated every t_m and the 2D potential force is updated every $\min(t_m,t_f)$. If $t_f > t_m$, which is the case in most situations, both forces are updated at t_m. If $t_f < t_m$, the Coulomb force is assumed to be constant during t_m and the 2D potential force is updated at t_f. The similar treatment is necessary for future consideration of a Lorentz force in a magnetic field, since the Lorentz force changes discontinuously after a scattering event where the direction of electron momentum

abruptly changes.

Finding an initial condition is not trivial because of the Coulomb interaction included. If any electrons are accidentally close to one another in the initial condition, this causes an artificial heating of the electron system; the average electron kinetic energy $\langle E_{\rm kin} \rangle$ should be equal to the thermal energy $k_B T$. We have performed a preliminary simulation to find an appropriate initial condition using a molecular-dynamics Monte Carlo code but with a slight modification. This modification consists of adding an operation to scale the momentum by $\sqrt{\langle E_{\rm kin} \rangle / k_B T}$ at every $\sim 10^2$ time step. Every time the scaling operation is performed, the average electron energy is reset to the thermal energy without changing the direction of momentum of each electron. This scaling perturbation is gradually turned off as the system approaches thermal equilibrium, since the scaling factor approaches unity. If the average kinetic energy shows essentially no time dependence, an appropriate initial condition is obtained. This preliminary simulation can start with any conditions with large enough kinetic energy. This is a computer version of the quenching experiment.

From an ensemble of real simulations with initial conditions found by the above method, the raw data consist of the position and momentum of each electron at each time step. Using these values, we can evaluate the velocity autocorrelation function $\langle v_x(i) v_x(0) \rangle$, the mean-square displacement $\langle \Delta x^2(i) \rangle$, and the radial distribution function $g(r)$. Since the thermal equilibrium states are simulated, we can take a time average as well as an ensemble average and this improves the statistical error in the results significantly. The basic practice is to gather as many data samples as possible. In order to evaluate $\langle v_x(i) v_x(0) \rangle$, an ensemble average of $v_x(i) v_x(0)$ over different electrons is available as usual. In addition to it, a time average $v_x(i+j) v_x(j)$ over different time j is available. Also, $\langle v_y(i) v_y(0) \rangle$ is available since the system is symmetric with respect to x and y. The same policy can apply to the mean-square displacement. Since the available number of samples decreases with increasing time index, these quantities for a long time comparable to the whole simulation time span have larger statistical error and need care. The evaluation of the radial distribution function $g(r)$ is straightforward in molecular dynamics since the distance for each pair of electrons is calculated every time step for the evaluation of the Coulomb potential and force. The gathered distances are averaged over ensemble and time to calculate $g(r)$. As a general guideline, data with more than $\sim 10^6$ samples are appropriate.

When evaluating a diffusion constant D, another quantity of interest, the usual method is to integrate the velocity autocorrelation function using Green-Kubo formula, by

$$D = \int_0^\infty \langle v_x(t) v_x(0) \rangle dt \ . \tag{10}$$

However, this method may not be suitable to the present simulations for the following reasons. First, the formula is for noninteracting particle systems and its applicability to the present case is questionable, in that the simulation computes only the single-particle correlation functions, and higher-order many-body terms may provide significant differences. Second, we need to perform a numerical integration and there is always a numerical error associated with this procedure even when good formulas are available. If the velocity autocorrelation function shows a long-lasting oscillation and the expected diffusion constant is close to zero, it is difficult to find a reasonable upper point of the integral. What is worse, the diffusion constant is not positive-definite in this definition. Third, the electron velocity changes discontinuously in a scattering event and this is not good for numerical calculations. Therefore we have created an Einstein plot of the mean-square displacement and evaluated the diffusion constant from its gradient, by[14]

$$D = \frac{1}{2} \frac{d}{dt} \langle \Delta x^2(t) \rangle \ . \tag{11}$$

The advantage of this method is the counterpoint of the above. First, it is the appropriate definition of the diffusion constant applicable even for interacting particles, and we can see whether the diffusion picture applies or not by checking the linearity of the Einstein plot. It gives a clear idea whether electrons are in the mobile phase, where $\langle \Delta x^2(t) \rangle$ increases linearly with time, or in an immobile phase where $\langle \Delta x^2(t) \rangle$ is bounded. Second, the numerical integration is avoided. Evaluating a derivative of the linear line is much easier than the numerical integration. Third, $\Delta x(t)$ changes continuously in a scattering event. After running several trial simulations, we have found the equivalence of (10) and (11) numerically, which has also been reported in molecular-dynamics calculations.[14,15] Once the numerical equivalence of these expressions is established, (11) is used extensively from thereon because of the advantage cited above.[16]

III. RESULTS AND DISCUSSION

A. Impurity and phonon scattering only

We start with the simplest case, which is the transport of free electrons at 4.2 K with only impurity and phonon scattering, where the impurity scattering dominates at this temperature. The impurities ($N_I = 3.3 \times 10^{15}$ cm^{-3}) are assumed to be uniformly distributed through the $Ga_{1-x}Al_xAs$ layer of the heterostructure, and we adopt the impurity screening model of Stern and Howard,[17] who formulated the impurity scattering in the context of electrons confined to the lowest subband of a FET structure. The inverse screening length is assumed to be $(nm/2\pi\hbar^2)(e^2/2\langle \varepsilon \rangle)$, where n is the areal electron density, $\langle \varepsilon \rangle$ is an average dielectric constant of GaAs and $Ga_{1-x}Al_xAs$, and the other symbols have their usual meanings.

Figure 2(a) shows the time evolution of the velocity autocorrelation function. The exponential dependence of the time is clearly shown in the figure, with a relaxation time τ of 4.6 ps. This value can be converted to the mobility $\mu = e\tau/m = 1.3 \times 10^5$ cm^2/V s, which corresponds to the diffusion constant $D = (k_B T/e)\mu = 46$ cm^2/s. Figure 2(b) shows the mean-square displacement of the elec-

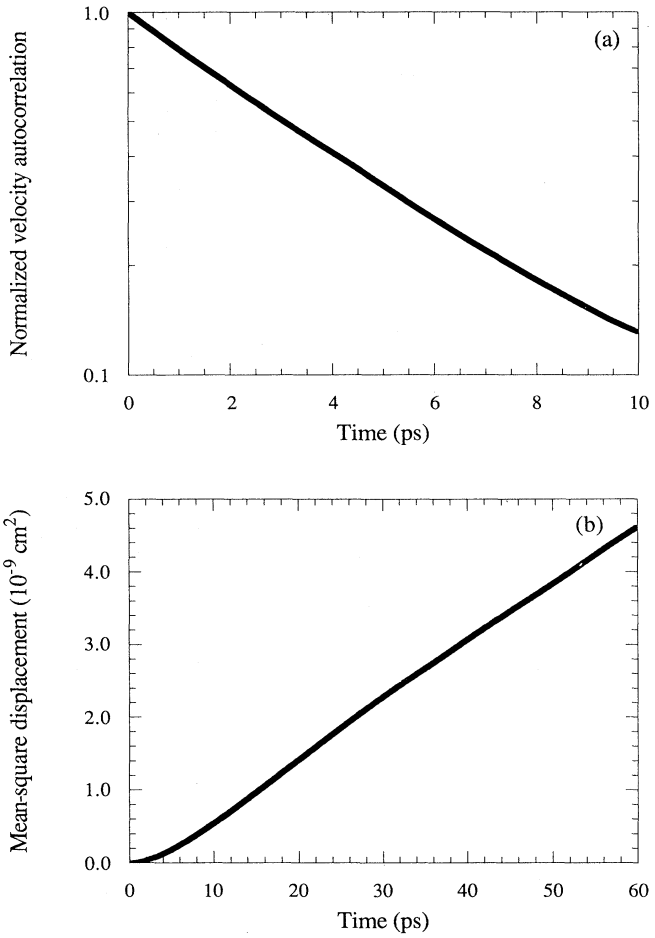

FIG. 2. The simulation result with only impurity and phonon scattering at 4.2 K. (a) The normalized velocity autocorrelation function of the particles as a function of time. (b) The mean-square displacement of the particles as a function of time.

trons. The linear dependence of the mean-square displacement on time immediately gives the diffusion constant of 42 cm^2/s. The difference defines the accuracy of the simulation, here about 10%, due to the small number of particles. The initial kinetic energy is conserved under elastic impurity scattering and, if the kinetic energy is chosen consistently with the temperature, it is maintained constant. Energy conservation on the computer is quite easily achieved in this case of the absence of the Coulomb interaction.

B. Impurity and phonon scattering, and electron-electron interaction with $V=0$

Next, electron-electron interaction is added to impurity and phonon scattering with the molecular dynamics. Now the system is regarded as a one-component 2D plasma and it is meaningful to make a connection to parameters often referred in plasma physics. The plasma coupling constant $\Gamma=e^2/(4\pi\varepsilon\lambda k_B T)$ is 6.43 in the present model, where $\lambda^{-1}=(\pi n)^{1/2}$ is the radius of the Wigner-Seitz disk and n is the areal density. It has been shown that there is a phase transition from a mobile phase to an immobile phase as Γ is increased, with a critical value of $\Gamma\sim 10^2$ in molecular-dynamics simulations.[18] The immobile phase is an ordered structure, known as a Wigner crystal, exhibiting a characteristic oscillation in the radial distribution function. Since the present value of Γ is much smaller than the critical value, electrons are in the mobile phase and possess a well-defined diffusion constant.

A remark has to be made about this phase transition. Mermin has published a rigorous proof that 2D systems cannot display long-range crystalline order.[19] The above statement may seem contradictory to this proof. However, the proof has two limitations. First, the interaction potential is assumed to fall off faster than r^{-2}. Second, the result only applies in the thermodynamic limit. The Coulomb potential falls off as r^{-1} and, obviously, the first condition is not satisfied. The second point is subtle, since we use a periodic boundary condition and the Ewald sum technique to eliminate unwanted boundary effects. In this sense, we are *virtually* simulating an infinitely large system. However, this is not mathematically equivalent to taking the thermodynamic limit. For these reasons, we can observe a phase transition in molecular-dynamics simulations which is not contradictory to Mermin's statement.

The velocity autocorrelation function changes drastically with the Coulomb interaction, as shown in Fig. 3(a). Two results, one with 32 electrons in 3×3 unit cells and the other with 14 electrons in 2×2 unit cells, are shown, where actually no LSSL is present ($V_0=0$) and the designations 2×2 and 3×3 are used only to specify the relative sizes of the simulation areas. Both show no essential difference and the original choice of 32 electrons in 3×3 unit cells seems reasonable. The velocity autocorrelation function is no longer a simple exponential function but an oscillatory function with a strong decay. Since the decay is quite strong, and numerical noise begins to merge into the autocorrelation function at around 4 ps, it is difficult to extract an oscillation period with good accuracy. In fact, the peak frequency depends on the choice of the window function in the numerical Fourier transform. With either a rectangular window or a Blackman window, an estimation gives the period as 3.2–3.7 ps.

The oscillation is attributed to the Coulomb interaction but the interpretation is not as easy as in the case of three-dimensional (3D) systems, where the oscillation is due to the coupling of a single electron to the plasma oscillations characterized by a frequency $\omega_{3D}=(e^2 n_{3D}/\varepsilon m)^{1/2}$, with n_{3D} the 3D electron density. This is a direct consequence of the fact that the charges are distributed on a plane, the simplest model for polarization in a 3D system, and create an electric field perpendicular to the plane with a strength that is independent of the distance from the plane. In 2D systems, however, the plasma oscillation has a dispersion that varies as $\sqrt{q}$. Actually, the polarization in 2D systems can be modeled by charges distributed on a line, creating an electric field inversely proportional to the distance from that line. Thus the squared plasma frequency, which is

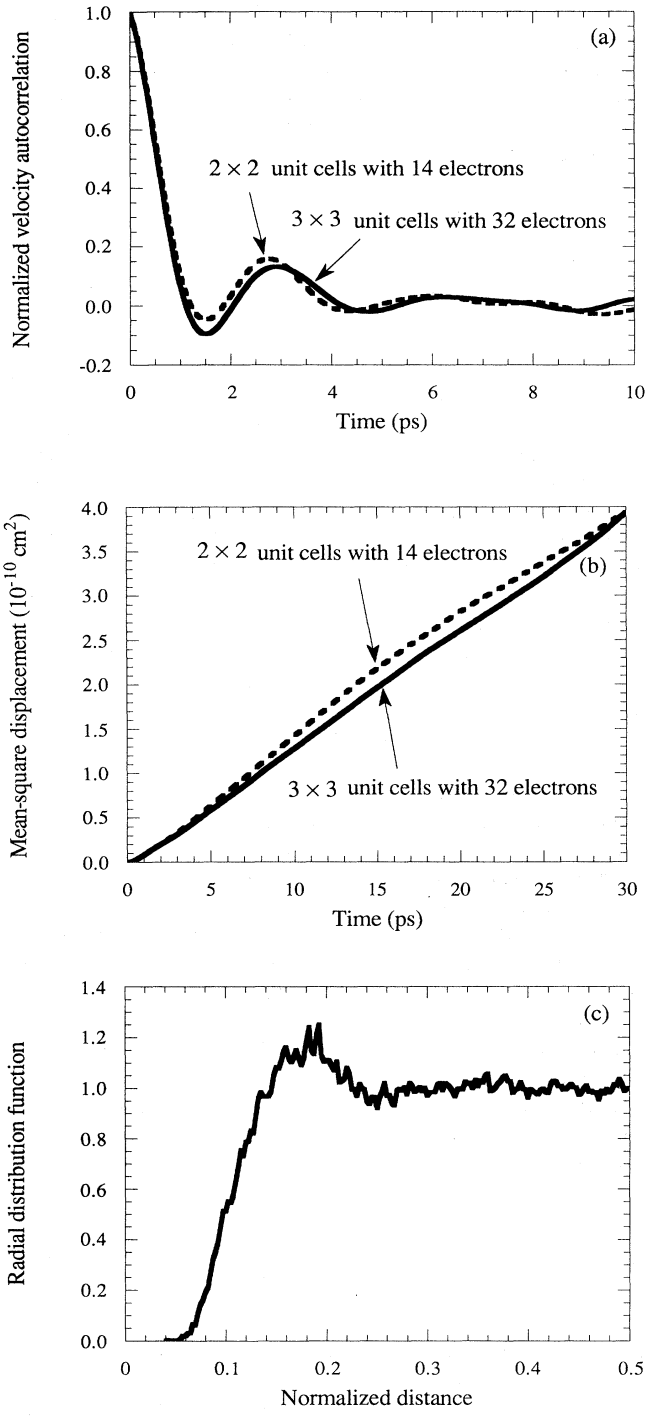

FIG. 3. The simulation result for the electron-electron interaction with impurity and phonon scattering present, but with $V_0=0$. The parameter is $\Gamma=6.43$ at 4.2 K. (a) The normalized velocity autocorrelation function. The solid line is the result for 32 electrons in a 3×3 unit cell and the dashed line that for 14 electrons in a 2×2 unit cell, although no superlattice potential is present. Here the designations 2×2 and 3×3 are used only to specify the size of the simulation area in terms of the basic lattice constant a. (b) The mean-square displacement of the particles. (c) The radial distribution function obtained for the 3×3 unit-cell simulation where the distance is normalized to L.

proportional to the field, is inversely proportional to the distance or proportional to q. The dispersion calculated in detail is $\omega_{2D}(q)=(e^2n_{2D}q/2\varepsilon m)^{1/2}$ in lowest order,[20] with n_{2D} the 2D electron density, which results in $\omega_{2D}(q)\rightarrow0$ when $q\rightarrow0$.

The situation seems puzzling, but it has been shown by several authors[21] that the oscillation in the velocity autocorrelation can be attributed to the 2D plasma oscillation with $q\sim q_0=(\pi n_{2D})^{1/2}$ rather than $q\sim0$, by studying the dynamic structure factor $S(q,\omega)$, which is directly calculated in molecular dynamics. The dispersion of the 2D plasma oscillation rises quickly with q and becomes almost flat around q_0,[21] showing a discrepancy from the curve $\omega=\omega_{2D}(q)$ due to higher-order effects that are automatically included in molecular dynamics. A 2D electron couples with this part of the mode, where the state density is large, and this is consistent with the fact that the 3D plasma oscillation has a flat dispersion part around $q\sim0$ and a 3D electron couples with this part. The time period corresponding to the flat part of the 2D plasma oscillation dispersion around q_0 is empirically given by $\sim5.2(4\pi\varepsilon m/e^2q_0^3)^{1/2}$,[15] which is estimated to be ~3.2 ps for the present situation of LSSL, consistent with our result of 3.2–3.7 ps.

Figure 3(b) shows the mean-square displacement under the condition of Fig. 3(a). Again, two results are shown, one with 32 electrons in 3×3 unit cells and the other with 14 electrons in 2×2 unit cells, exhibiting no essential difference. Since the figure shows a clear linear dependence on time, we can still use a diffusion picture of Brownian particles although electrons are interacting through the Coulomb force. The diffusion constant D is evaluated to be 6.7 cm^2/s, which is smaller than the value with impurity scattering only. Usually, the Coulomb interaction conserves the total momentum of the electron system and therefore does not change the transport properties. However, the present result is a natural conclusion if we remember that the phase transition from the mobile to the immobile phase occurs as Γ increases. The result for larger Γ will be discussed later.

Figure 3(c) shows the radial distribution function for $V_0=0$ obtained from the 3×3 unit-cell simulation. The distance is normalized to L. The radial distribution has essentially zero value for short distances but rises rapidly and peaks around $1/\sqrt{32}=0.177$, which is the average distance assuming a perfectly uniform 2D electron gas. As the distance increases, the radial distribution function approaches unity without showing an oscillation. This is further evidence that the electrons are in a uniform, mobile phase. The initial peak in the radial distribution function is larger than unity and this indicates an effective attraction in the system. The origin of the attraction is the same as that of hard-sphere systems and can be intuitively understood as follows. When the second electron is at a distance corresponding to this region from the central electron, there is little possibility of inserting a third electron between them since electrons cannot approach within a certain distance due to the strong Coulomb repulsive force, just as the third electron cannot find enough space to enter in hard-sphere systems. As a result, the second electron suffers less scattering

from other electrons on the side facing the central electron than from those on the opposite side: the effect is a net average attraction toward the center.

Since the initial condition is properly chosen, the average kinetic energy with respect to time is the temperature 0.36 meV. Slight oscillations in energy about this value are observed with time. They are due to the 2D plasma oscillation and attributed to the finite number of electrons used in the simulation. If the number of electrons N increases, the fluctuations decrease as $1/\sqrt{N}$ and go to zero in the infinite limit. Although there are some oscillations in energy, the total energy stays essentially constant during the simulation.

In order to assure the validity of the minimum image approximation for the Coulomb interaction under the present condition, one simulation has been performed under the condition that the Coulomb interaction is more dominant—a larger Γ case. The temperature is assumed to be the same, 4.2 K, but the side of the area is decreased so that Γ will be 36. This is a mathematical test rather than a physical one, to check whether the minimum image approximation gives essentially the same result as those of the more exact Ewald sum treatment. The oscillation of the velocity autocorrelation becomes clearer, as shown in Fig. 4. By taking the Fourier transform, the time period for this oscillation is estimated to be 0.20–0.22 ps, which is consistent with the value of 0.20 ps assuming the coupling of a single electron to the 2D plasma oscillation at $q \sim (\pi n)^{1/2}$. The mean-square displacement shows a linear dependence on time after ~ 1.5 ps, and the displacement after that is fitted to a straight line to evaluate the diffusion constant D. This gives $D \sim 4.3$ cm^2/s. The reported value was $D = 5.1$ cm^2/s for $\Gamma = 36$.[12] If we use Matthiessen's rule to include the effect of impurity scattering using the diffusion constant determined by impurity scattering alone, the reported value is changed to 4.6 cm^2/s. Thus the minimum image approximation agrees with results of a more exact Ewald sum treatment for $\Gamma = 36$ and is appropriate for the present model. The Coulomb interaction is so dominant over the thermal fluctuation of the electrons that their spatial distribution begins to show some order, which is conducive to reducing Coulomb energy as is indicated in the peaks of the radial distribution function.

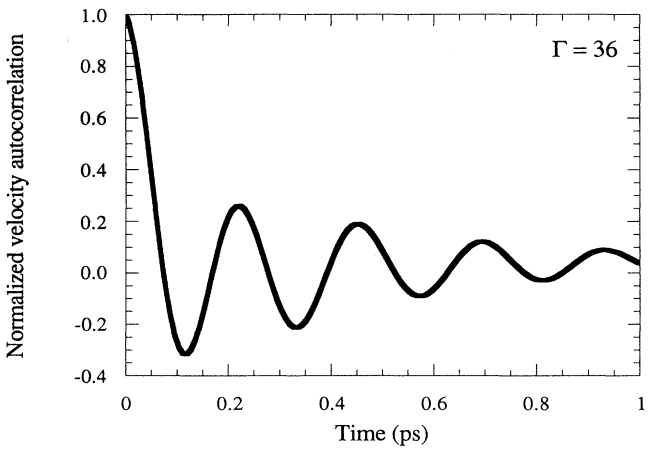

FIG. 4. The normalized velocity autocorrelation function of electrons for plasma coupling constant $\Gamma = 36$, realized with a higher electron density at the same temperature 4.2 K under the electron-electron interaction with impurity and phonon scattering.

C. Addition of 2D periodic potential

Next we consider the 2D potential. With increasing 2D periodic potential, electrons tend to stay at the potential minima and, if the potential exceeds some critical value, electrons will show a phase transition from a mobile to an immobile phase. This can also be understood by checking the average value of the sum of the kinetic energy and 2D potential energy. If this value is greater than the saddle-point energy of the 2D potential, which is the lowest 2D potential barrier energy, electrons can move anywhere in space. Otherwise, most electrons are confined in a unit cell and only some gain enough energy to overcome the saddle point and move to neighboring cells, leading to a smaller diffusion constant. This is reminiscent of classical hopping, leading to a smaller diffusion constant. With greater potential, no electrons can change their original cells, resulting in zero diffusion constant.

These insights are actually seen in the results. Figure 5(a) shows the velocity autocorrelation for three potential values, 2.5, 5, and 10 meV. The velocity autocorrelation function begins to show an oscillation with a shorter time period than that in the presence of the Coulomb interaction alone seen above. This oscillation can be attributed to classical oscillation in the potential. For $V_0 = 10$ meV, a clear oscillation is observed, which indicates that electrons are beginning to be confined in the potential minima and that the major force dominating electron motion is changing from a Coulomb force to a 2D potential force. The Fourier transform of the velocity autocorrelation function for $V_0 = 10$ meV shows a peak corresponding to the time period of 2.2 ps. Generally, the time period T_{class} in the classical periodic motion of a particle with mass m in the one-dimensional potential well $U(x)$ can be given by

$$T_{\text{class}} = 2\int_{x_1}^{x_2} dx \frac{1}{\sqrt{2[E - U(x)]/m}} , \tag{12}$$

where $E = \langle E_{\text{kin}} \rangle$ and x_1 and x_2 are the classical turning points where $U(x) = E$. Along the minimal potential line in the y direction given by $\cos(2\pi y/a) = -1$, we can express the motion in the x direction in the present problem by

$$T_{\text{class}} = 4a \left[\frac{m}{2V_0} \right]^{1/2} \times \int_{\theta_1}^{1/2} d\theta \frac{1}{\left[\frac{E}{V_0} - \frac{\cos(2\pi\theta)+1}{4} \right]^{1/2}} , \tag{13}$$

where $\theta_1 = x_1/a$ and x_1 is the classical turning point with $0 < x_1 < a/2$. The divergence of the integrand at the

turning point is like $(\theta-\theta_1)^{-1/2}$ and integrable as long as $\theta_1 \neq 0$ or E is smaller than the saddle-point energy. The numerical integration with $E=k_B T=0.362$ meV and $V_0=10$ meV gives $\theta_1=0.413$ and $T_{\text{class}}=2.43$ ps, which recovers the observed value.

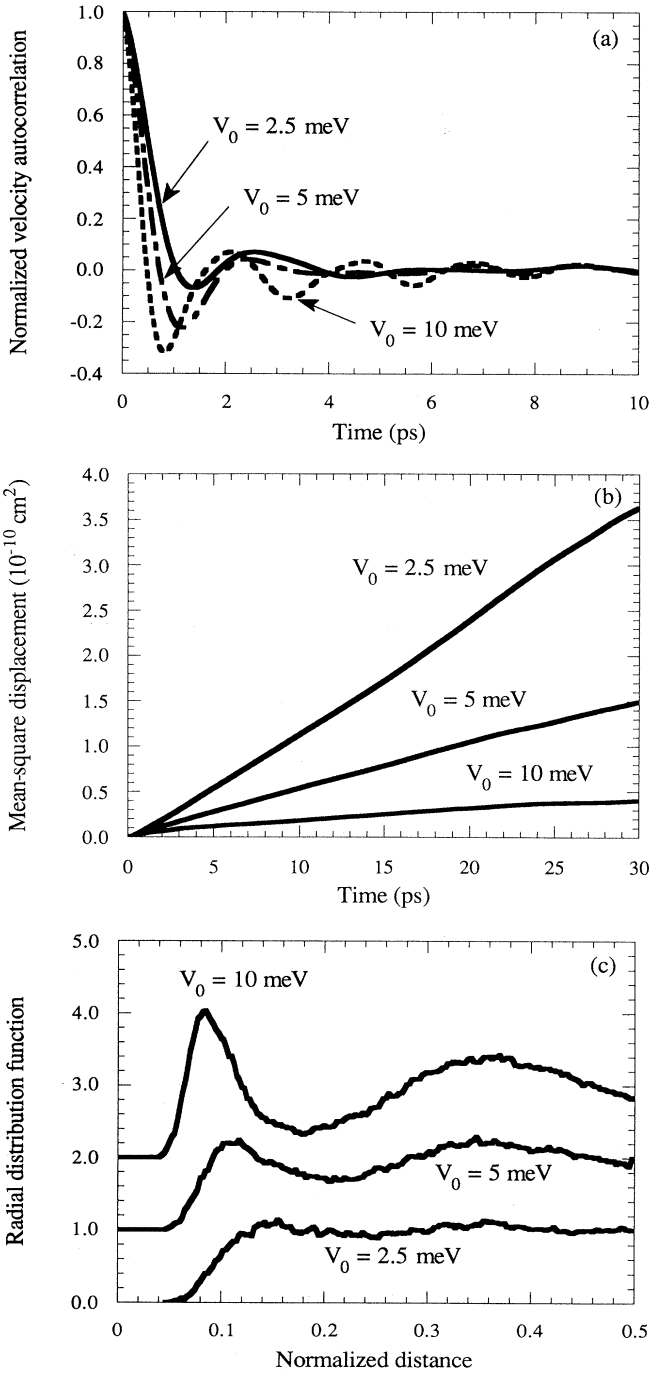

FIG. 5. Simulation results for the potential amplitude $V_0=2.5$, 5, and 10 meV under the electron-electron interaction with impurity and phonon scattering at 4.2 K. (a) The normalized velocity autocorrelation function. (b) The mean-square displacement. (c) The radial distribution function where the distance is normalized to L.

Figure 5(b) shows the mean-square displacement for $V_0=2.5$, 5, and 10 meV. We have a linear time dependence of the mean-square displacement, indicating that electrons are still in the mobile phase, although the oscillation in the velocity autocorrelation has already shown that the electron confinement at the bottom of the potential minima is beginning. From the figure, we can estimate the diffusion constant as $D=6.1$ cm^2/s for $V_0=2.5$ meV, $D=2.5$ cm^2/s for $V_0=5$ meV, and $D=0.6$ cm^2/s for $V_0=10$ meV.

These situations become clearer by checking the relation of the saddle-point energy and the sum of electron kinetic and 2D potential energy. For $V_0=2.5$ meV, the saddle-point energy $V_0/2$ is smaller than the sum. Most electrons can overcome the 2D potential barrier and are not confined in a unit cell. However, this relation reverses at $V_0=5$ meV and a majority of electrons now do not have enough energy to overcome the barrier and are confined in a unit cell. Coulomb energy increases with potential, which is another manifestation that electrons are gradually confined in a cell, since spatially nonuniform distribution will raise Coulomb energy.

Figure 5(c) shows the radial distribution function for three potential values. For clarity, the functions for $V_0=5$ and 10 meV are offset by one and two units. The first peak of the distribution function shifts to a smaller distance with increasing potential, due to the increasing confining effect in a unit cell. The electrons do not prefer to stay around the normalized distance of $\frac{1}{6}$, where the potential barrier appears, with increasing potential. The second peak for the normalized distance of $\frac{1}{3}$ becomes higher and corresponds to the 2D potential period, further indicating confinement.

The situation changes drastically for $V_0=40$ meV, since electrons have already made a phase transition to the localized state. Electrons oscillate at the bottom of the potential minima and none can overcome the barrier. The velocity autocorrelation in Fig. 6(a) has a clear oscillation period. The Fourier-transform amplitude has a peak at the frequency corresponding to a time period of 1.1 ps. Using the expression in (13) with $V_0=40$ meV, we have $\theta_1=0.457$ and $T_{\text{class}}=1.10$ ps. The mean-square displacement in Fig. 6(b) is a bounded function of time and therefore the diffusion constant is zero. The sum of average kinetic and 2D potential energy is around 3.3 meV, which is much smaller than the saddle-point energy of 20 meV. Practically, it is impossible for electrons to overcome the barrier at this low temperature of 4.2 K. Coulomb energy achieves the highest contribution because of the strong spatial confinement of electrons in the potential minima. This is why the radial distribution function in Fig. 6(c) shows a high first peak corresponding to the mean distance of electrons in a unit cell, followed by an essentially zero region due to high potential barrier, and the second peak corresponds to the 2D potential period at the normalized distance of $\frac{1}{3}$. The third peak at the normalized distance at $\sqrt{2}/3$ is essentially the manifestation of the 2D square-ordered structure in the diagonal direction.

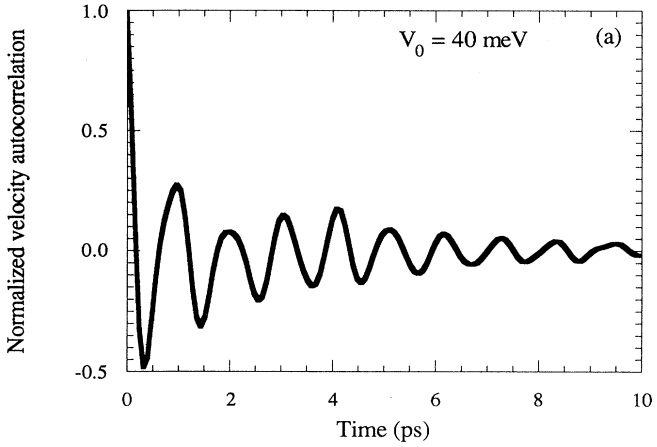

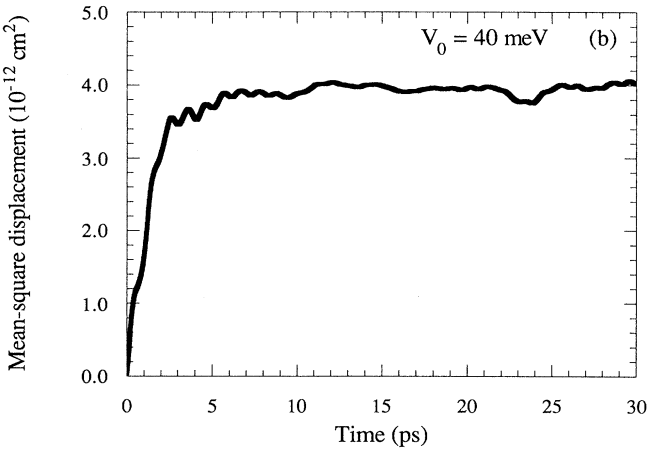

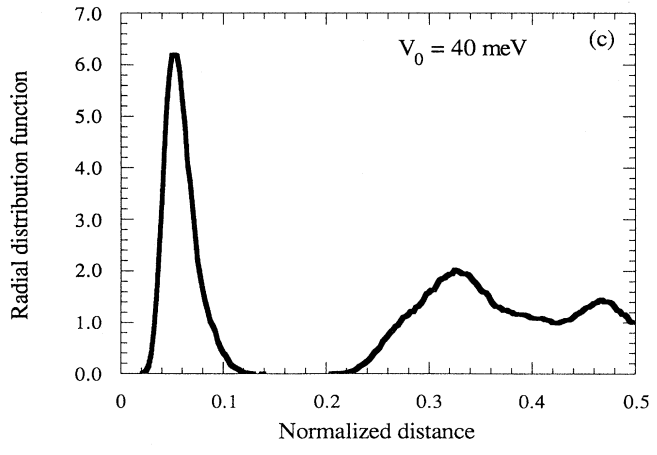

FIG. 6. Simulation results for the potential amplitude $V_0=40$ meV under the electron-electron interaction with impurity and phonon scattering at 4.2 K. (a) The normalized velocity autocorrelation function. (b) The mean-square displacement. (c) The radial distribution function where the distance is normalized to L.

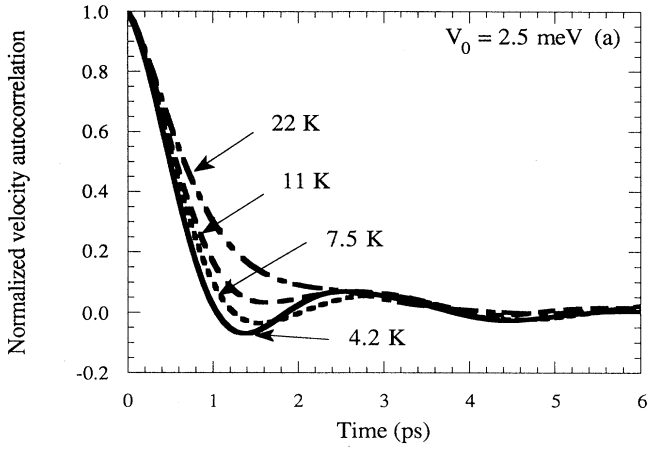

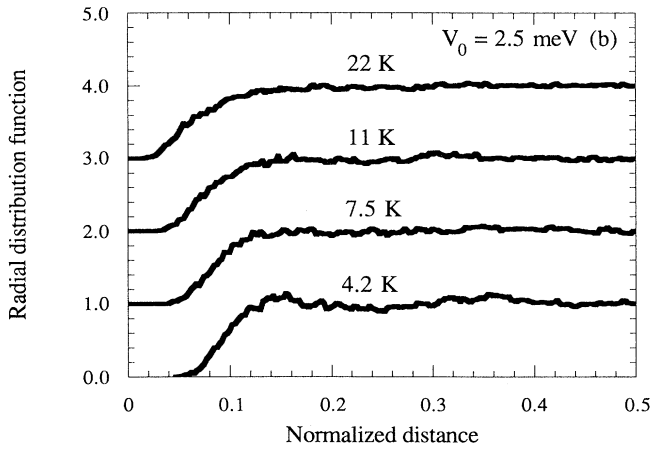

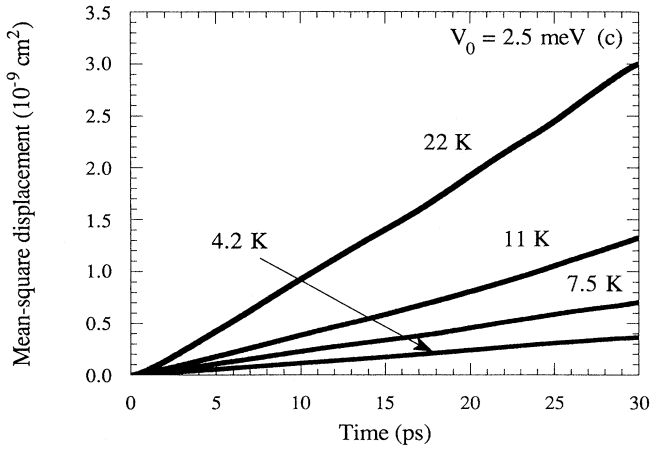

FIG. 7. Simulation results for $V_0=2.5$ meV under the electron-electron interaction with impurity and phonon scattering at various temperatures. (a) The normalized velocity autocorrelation function. (b) The radial distribution function where the distance is normalized to L. (c) The mean-square displacement.

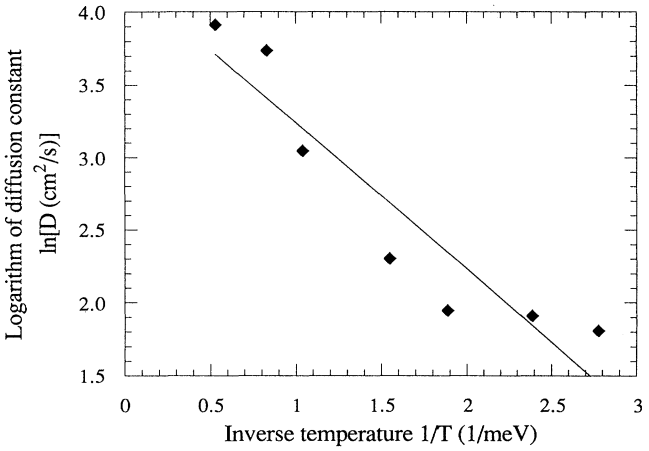

FIG. 8. The plot of the natural logarithm of the diffusion constant ($\ln D$) as a function of inverse temperature ($1/T$). The estimated activation energy is ~ 1.0 meV.

D. Effect of temperature

The effect of raising the temperature is obvious. As long as phonon scattering remains small, a higher temperature causes improvement in transport since electrons have more energy to overcome the 2D potential barrier or Coulomb potential barrier. In order to show this, we have simulated several temperature points between 4.2 and 22 K for $V_0 = 2.5$ meV. Figure 7(a) shows the velocity correlation function, Fig. 7(b) the radial distribution function, and Fig. 7(c) the mean-square displacement, for several temperatures. The velocity autocorrelation function begins to show a simple monotonic decay, rather than an oscillation, with increasing temperature. With increasing kinetic energy, the coherent collective oscillation is disturbed and the oscillation in the velocity autocorrelation function becomes weaker. With increasing temperature, the radial distribution function approaches that of noninteracting particles. The diffusion constant also grows with temperature. By creating a plot of $\ln(D)$ versus inverse temperature $1/T$, we can estimate an activation energy, as shown in Fig. 8. By calculating the gradient, the activation energy is ~ 1.0 meV, on the order of V_0.

IV. CONCLUSION

We have studied the transport properties of LSSL's with a molecular-dynamics Monte Carlo technique including the Coulomb interaction. Excellent numerical energy conservation is achieved by using the predictor-corrector algorithm to integrate the equation of motion. With increasing 2D potential amplitude, electrons show a transition from a mobile phase of the electron gas, where only short-range order is formed, to an immobile phase where the radial distribution function has some characteristic peaks, indicating the localization of the particles. The velocity autocorrelation function in the mobile phase shows a 2D plasma oscillation, while in the localized phase it exhibits a classical oscillation at the bottom of the potential well. Raising the temperature improves transport, since electrons are released from the constraint of the 2D potential or the Coulomb potential. The simulation clearly illustrates the activated conductance in this system.

ACKNOWLEDGMENTS

The authors are grateful to A. M. Kriman for useful discussions. This work was supported by the Office of Naval Research.

[1]See, e.g., Phys. Today, the special issue on Nanoscale and Ultrafast Devices, February (1990); *Granular Nanoelectronics,* edited by D. K. Ferry, J. R. Barker, and C. Jacoboni (Plenum, New York, 1990); *Nanostructure and Mesoscopic Systems,* edited by W. P. Kirk and M. A. Reed (Academic, San Diego, 1991); C. W. J. Beenakker and H. van Houten, in *Solid State Physics,* edited by H. Ehrenreich and D. Turnbull (Academic, San Diego, 1991), Vol. 44.

[2]E. Paris, J. Ma, A. M. Kriman, D. K. Ferry, and E. Barbier, J. Phys. Condens. Matter **3**, 6605 (1991); J. Ma, R. A. Puechner, W.-P. Liu, A. M. Kriman, G. N. Maracas, and D. K. Ferry, Surf. Sci. **229**, 341 (1990).

[3]D. Weiss, K. v. Klitzing, K. Ploog, and G. Weimann, Europhys. Lett. **8**, 179 (1989); C. W. J. Beenakker, Phys. Rev. Lett. **62**, 2020 (1989).

[4]C. W. J. Beenakker and H. van Houten, Phys. Rev. Lett. **63**, 1857 (1989).

[5]D. Weiss, M. L. Roukes, A. Menschig, P. Grambow, K. v. Klitzing, and G. Weimann, Phys. Rev. Lett. **66**, 2790 (1991).

[6]P. Lugli and D. K. Ferry, Appl. Phys. Lett. **46**, 594 (1985); Phys. Rev. Lett. **56**, 1295 (1985); D. K. Ferry, *Semiconductors* (Macmillan, New York, 1991).

[7]The tradeoff between thermal energy and the Fermi energy in a quasi-two-dimensional gas has been discussed in connection with screening by F. Stern and W. E. Howard, Phys. Rev. **163**, 816 (1967). These authors point out that the screening is little different from the nondegenerate Debye limit for the conditions considered here, and the Fermi energy must be considerably larger than the thermal energy before a transition to Fermi-Thomas screening is necessary. Here, the Fermi energy is sufficiently small that the thermal spread of the Fermi-Dirac distribution cannot be distinguished from its classical counterpart.

[8]One might assume that since the system is near degeneracy, the exchange potential modifications to the Coulomb interaction should be included within the molecular dynamics. This has been done previously by A. M. Kriman, M. J. Kann, D. K. Ferry, and R. Joshi, Phys. Rev. Lett. **65**, 1619 (1991). The modifications that arise from the exchange interaction are only of importance at very high densities, and play no role for the small densities considered here.

[9]F. F. Fang and W. E. Howard, Phys. Rev. Lett. **16**, 797 (1966);

F. Stern, Phys. Rev. B **5**, 4891 (1972).

[10]P. J. Price, Ann. Phys. (N.Y.) **133**, 217 (1981).

[11]It should be pointed out that the assumption of periodic boundary conditions does not truncate the Coulomb potential at these boundaries. Rather it, and the minimum image approximation, only assures that the force calculations are made with the nearest images of the repetitive cells, thus avoiding any erroneous average force arising from an off-centered set of image particles. In essence, these techniques assume that the particle at which the force is calculated sits at the center of its own unit cell; see, e.g., M. J. Kann, A. M. Kriman, and D. K. Ferry, Phys. Rev. B **41**, 12 659 (1990), and references therein.

[12]M. P. Allen and D. J. Tildesley, *Computer Simulation of Liquids* (Clarendon, Oxford, 1987).

[13]D. J. Adams and G. S. Dubey, J. Comp. Phys. **72**, 156 (1987).

[14]P. J. Price, in *Fluctuation Phenomena in Solids,* edited by R. E. Burgess (Academic, New York, 1965), pp. 355–380; B. J. Alder and T. E. Wainright, Phys. Rev. A **1**, 18 (1970).

[15]J. P. Hansen, D. Levesque, and J. J. Weis, Phys. Rev. Lett. **43**, 979 (1979).

[16]One might naively think that this is the diffusion of a test particle. However, this self-diffusion of the carriers is precisely the diffusion constant related to the mobility by the fluctuation-dissipation theorem [see, e.g., R. Kubo, in *Transport Phenomena,* edited by J. Ehlers, K. Hepp, and H. A. Weidenmüller (Springer-Verlag, Berlin, 1974), pp. 75–125], and is normally used in computing the transport properties by ensemble Monte Carlo techniques at low values of the drift field, as is discussed by C. Jacoboni and L. Reggiani, Rev. Mod. Phys. **65**, 645 (1983).

[17]F. Stern, Phys. Rev. Lett. **18**, 546 (1967); see also the reference to Stern and Howard in Ref. 7 above.

[18]R. C. Gann, S. Chakravarty, and G. V. Chester, Phys. Rev. B **20**, 326 (1979).

[19]N. D. Mermin, Phys. Rev. **171**, 272 (1968).

[20]C. C. Grimes, Surf. Sci. **73**, 379 (1978); T. Ando, A. B. Fowler, and F. Stern, Rev. Mod. Phys. **54**, 437 (1982).

[21]H. Totsuji and H. Kakeya, Phys. Rev. A **22**, 1220 (1980); R. K. Kalia, P. Vashishta, S. W. de Leeuw, and A. Rahman, J. Phys. C **14**, L911 (1981).